International Journal of Solids and Structures 47 (2010) 3447–3461

Contents lists available at ScienceDirect

International Journal of Solids and Structures

journal homepage: www.elsevier.com/locate/ijsolstr

Formulation of the high-fidelity generalized method of cells with arbitrary cell geometry for refined micromechanics and damage in composites

Rami Haj-Ali *[,1], Jacob Aboudi

School of Mechanical Engineering, Faculty of Engineering, Tel-Aviv University, Ramat-Aviv 69978, Israel

ARTICLE INFO

Article history:
Received 11 March 2010
Received in revised form 27 July 2010
Available online 8 September 2010

Keywords:
Micromechanical analysis
High-fidelity generalized method of cells
Multiphase composites
Arbitrary geometry
Parametric variables
Progressive damage

ABSTRACT

A new parametric formulation for high-fidelity generalized method of cells (HFGMC) is presented for the micromechanical analysis of multiphase periodic composites. To this end, a linear parametric and geometric mapping is employed to transform arbitrary quadrilateral cell shapes from the physical space to an auxiliary uniform square shapes. A complete quadratic displacement expansion is performed in the mapped space. Thus, a new bilinear term is added to the quadratic displacement expansion; unlike the original HFGMC for regular array of rectangular cells where this term in not required. The continuity of displacements, tractions, together with the periodicity and equilibrium conditions are imposed in the average sense, similar to the original HFGMC formulation, using both the physical and mapping variables. However, the addition of bilinear terms requires the introduction of the first averaged moments of the equilibrium equations. In order to demonstrate the ability the new HFGMC formulation, spatial stress fields are compared with analytical and numerical solutions of circular and elliptical fibers in an infinite medium. Furthermore, two progressive damage methodologies are coupled with the new HFGMC formulation in order to predict the strain softening and elastic degrading behaviors. The first methodology employs a cell extinction approach, while the second uses cohesive interfaces between the cells. Due to the strain softening, both damage methodologies require an iterative solution approach of the governing system nonlinear equations. Damage applications are presented for the transverse loading of composites with square and hexagonal repeating unit-cells (RUC).

1. Introduction

A major challenge in the micromechanical analysis of multiphase composite materials is the accurate geometrical representation of the phases and microstructure. Accurate prediction of the spatial distributions of local fields requires a refined depiction of the geometry of the microstructure. Classical micromechanical theories are successful in generating both effective linear and nonlinear response. This is because the exact geometrical representation of the constituents has a higher-order effect on the effective behavior. However, a refined micromechanical analysis is needed whenever the detailed spatial distribution of the local fields is required, such as the stress concentration near voids and material imperfections. Furthermore, proper prediction for the initiation and progression of inelastic and damage effects can also require refined micromechanical analysis.

The HFGMC micromechanical theory can be employed for the refined nonlinear analysis of multiphase composites, Aboudi (2004). It provides a viable alternative to classical numerical methods such as finite element (FE) and finite difference. This is because it is directly specialized and geared towards multiphase composites as its formulation is explicitly based on micromechanical variables needed to establish the elastic and inelastic concentration tensors of the phases in addition to the detailed local fields. The HFGMC method has evolved from its predecessors, the method of cells (MOC) and the generalized method of cells (GMC), Aboudi (1989, 1991), Paley and Aboudi (1992), respectively. The HFGMC employs higher-order displacement expansion whereas in MOC and GMC the displacement expansion is limited to a linear one.

Several recent re-formulations of the HFGMC have been conducted. Haj-Ali and Aboudi (2009) provided total and incremental formulation of the HFGMC for the micromechanical analysis of nonlinear multiphase materials. To this end, an iterative procedure has been developed to minimize the residual error and satisfy the HFGMC governing equations in their total form. In Aboudi (2002), a finite strain HFGMC formulation has been performed for the analysis of composites undergoing large deformations. This necessitates the use of conjugate stress and strain measures along with the deformation gradient tensor. Various types of finite strain constitutive equations have been implemented within the finite strain

* Corresponding author. Tel.: +972 3 640 8207; fax: +972 3 640 7617.
E-mail address: rami98@eng.tau.ac.il (R. Haj-Ali).
[1] On leave from Georgia Institute of Technology, Atlanta, GA 30332, USA.

0020-7683/$ - see front matter © 2010 Elsevier Ltd. All rights reserved.
doi:10.1016/j.ijsolstr.2010.08.022

HFGMC framework such as hyperelastic coupled with damage, thermo-inelastic and thermo-viscoelastic, see an expanded review by Aboudi (2008). Bansal and Pindera (2004) provided a re-formulation for the linear elastic HFGMC by directly employing the cell average displacements as the sole independent variables which enables variable condensation, thus enhances the computational efficiency. This same approach is followed by Bansal and Pindera (2006), using this HFGMC method, to include plasticity effects. Although this case is also a direct implementation of the HFGMC method; it was renamed by these authors.

The HFGMC method has been extensively applied over the last decade. Coupled electro-magneto-thermo-elastic analysis of multiphase composites have been studied (Aboudi, 2001). Inelastic and viscoelastic–viscoplastic micromechanical effects have been investigated using the HFGMC by Aboudi et al. (2003) and Aboudi (2005). Interfacial damage and fiber loss effects using HFGMC were addressed by Bednarcyk et al. (2004) and Ryvkin and Aboudi (2007). The analysis of periodic lattice blocks has been performed by Aboudi and Gilat (2005), whereas pressurized foam cell microstructure in the insulation of the external tank of the space shuttle have been carried out by Bednarcyk et al. (2008). Numerous types of smart composite material systems have been modeled using the HFGMC method, see Aboudi (2007) for an extensive review. In the area of shape memory alloy composites the HFGMC has been extended and applied to the local and global behavior of these material systems, see the recent study of Freed and Aboudi (2009). Finally, Bruck et al. (2007) employed the HFGMC modeling capability in the optimization of porous microstructures using multi-objective function with the genetic algorithm method.

The current HFGMC formulation has to be performed on orthogonal arrays of cells used to model the geometry of the phases. This limitation requires a relatively large cell number in order to accurately capture refined geometrical features. Despite this limitation, the previous applications have demonstrated the effectiveness of the method to generate the local field solutions when using sufficiently large number of cells. It should be emphasized that few number of rectangular cells is sufficient to generate the effective linear and nonlinear response with high accuracy. In fact, this is one of the advantages of using the HFGMC in a local–global analysis of composite structures (Haj-Ali and Aboudi, 2009).

In order to overcome the aforementioned limitation, a linear geometrical mapping of cells is proposed. Towards this goal, quadrilateral shape cells are used to map the phases and microstructures of the composite. This linear and parametric geometric mapping can be arbitrarily applied for general phase geometry using quadrilateral cell shapes that are transformed to an auxiliary uniform square shape. It is important to note that while linear geometric mapping is employed, quadratic displacement expansion, similar to the original HFGMC, is still performed but in the auxiliary space coordinate system. Special attention is made to employ a complete quadratic polynomial expansion in the auxiliary space in order apply the proper mapping for arbitrary cell geometry.

This paper is organized as follows. Section 2 presents the general re-formulation of the HFGMC with linear mapping including the establishment of the concentration and the effective stiffness tensors. The last part of this section deals with the global HFGMC system of equations represented in a compact form which facilitates an efficient iterative solution. Section 3 is concerned with damage formulation in conjunction with the HFGMC and its linear mapping. Two progressive damage methods are introduced. The first is based on cell extinction approach while the second employs cohesive modeling at the interfaces between the cells. Section 4 presents applications and verifications of the theory. A general discussion can be found in Section 5, followed by conclusions in Section 6.

2. General formulation

The HFGMC micromechanical method has been developed for the analysis of multiphase composite materials. Fig. 1 schematically illustrates a periodic multiphase material system having a global coordinates (x_2,x_3). The repeating unit-cell (RUC) of this medium is identified and described with respect to the coordinate system (Y_2,Y_3). The HFGMC method is based on the homogenization technique for periodic composites and is capable of predicting the spatial local deformation field as well as the overall effective behavior. In the framework of this method, the RUC is divided into regular array of cells, often denoted as subcells. In the present section, this method is extended to analyze an RUC with a irregular array of generally shaped quadrilateral cells. Fig. 2(a) and (b) shows the RUC domain which is discretized into a general assembly of quadrilateral cells to represent the different phase geometries. In addition, a general quadrilateral cell is isolated and shown in its physical coordinates (y_2,y_3), Fig. 2(c), whose origin is located at the center of the cell. This cell is mapped to a uniform parametric coordinate system (r,s) using the classical linear transformation

$$y_2(r,s)=\sum_{i=1}^{4}H_i(r,s)y_2^{(i)},\quad y_3(r,s)=\sum_{i=1}^{4}H_i(r,s)y_3^{(i)} \tag{1}$$

where

$$\begin{aligned} H_1&=\frac{1}{4}(1-r)(1-s),\quad H_2=\frac{1}{4}(1+r)(1-s)\\ H_3&=\frac{1}{4}(1+r)(1+s),\quad H_4=\frac{1}{4}(1-r)(1+s)\end{aligned} \tag{2}$$

and $(y_2^{(i)},y_3^{(i)})$ are the corner coordinates of the cell.

As in the original HFGMC formulation (e.g., Aboudi, 2004), the displacement field in the physical coordinates of the cell is expanded in the form:

$$\begin{aligned}\mathbf{u}=\boldsymbol{\epsilon}^0\cdot\mathbf{x}+\mathbf{W}_{(00)}+\mathbf{W}_{(10)}y_2+\mathbf{W}_{(01)}y_3+\frac{1}{2}\mathbf{W}_{(20)}\left(3y_2^2-\frac{h^2}{4}\right)\\ +\frac{1}{2}\mathbf{W}_{(02)}\left(3y_3^2-\frac{l^2}{4}\right)\end{aligned} \tag{3}$$

where $\boldsymbol{\epsilon}^0$ is the externally applied average strain with h and l are the cell dimensions. The coefficient variables vectors, $\mathbf{W}_{(mn)}$, represent the volume averaged displacement in the case of $m=n=0$, which together with the additional higher-order terms have to be determined.

Expansion (3) is suitable for regular and orthogonal array of cells. However, the above displacement expansion form is not suitable for a general quadrilateral cell geometry. Attempts to identically use the above polynomial to reformulate the HFGMC for irregular and general cell geometries have been conducted by Khatam and Pindera (2009). The missing bilinear term, $y_2y_3W_{(11)}$ in Eq. (3), is required in order to achieve completeness and proper transition from the linear to the full quadratic order. This requirement is well-known in the mathematical literature as the Pascal Triangle. In addition, the choice of interpolation terms and functions has been extensively discussed in the finite-element literature whereby improper transition can lead to undesirable effects such as gaps and overlaps between adjacent cells. A more expanded discussion of these effects can be found in Cook et al. (2002), for example.

A general parametric expansion of the displacement in the cell, using the auxiliary parametric coordinates (r,s), can be expressed using the Legendre polynomials as follows

$$\mathbf{u}=\boldsymbol{\epsilon}^0\cdot\mathbf{x}+\sum_{m=0}^{M}\sum_{n=0}^{N}\mathbf{W}_{(mn)}P_m(r)P_n(s) \tag{4}$$

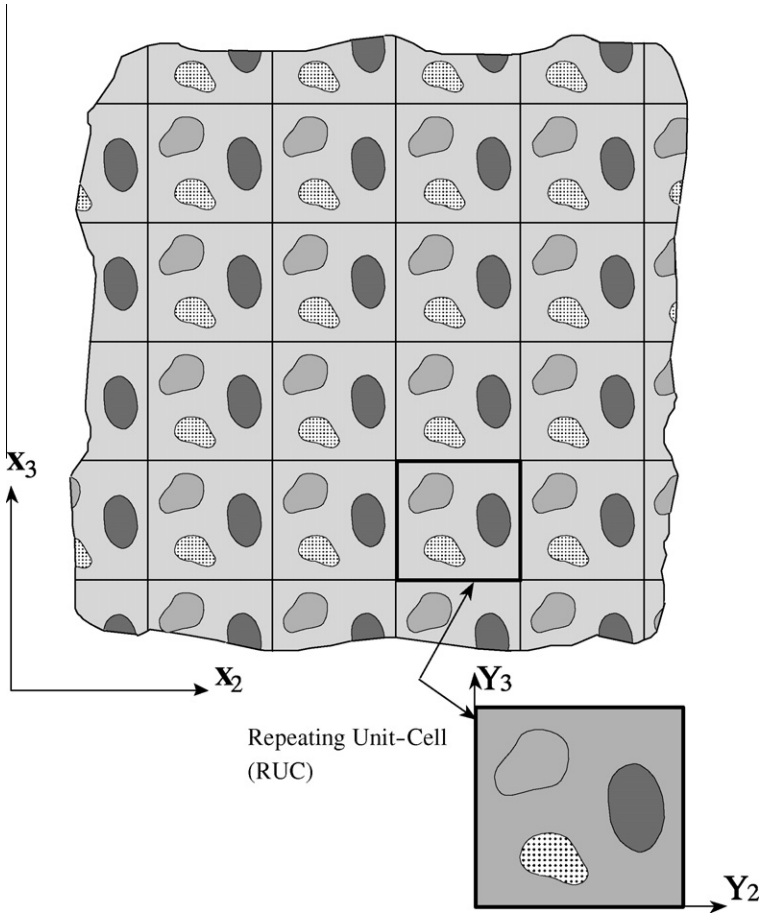

Fig. 1. Schematic illustration of a unidirectional periodic array in the global $(x_2 - x_3)$ plane of multiphase composite media with its repeating unit-cell (RUC), defined with respect to its $(Y_2 - Y_3)$ local coordinate system.

In the present HFGMC formulation the proper complete quadratic form is given by

$$\mathbf{u} = \boldsymbol{\epsilon}^0 \cdot \mathbf{x} + \mathbf{W}_{(00)} + \mathbf{W}_{(10)} r + \mathbf{W}_{(01)} s + \mathbf{W}_{(11)} rs + \frac{1}{2}\mathbf{W}_{(20)}(3r^2 - 1) + \frac{1}{2}\mathbf{W}_{(02)}(3s^2 - 1) \tag{5}$$

The mapping between the parametric and physical cell geometries is performed using the above transformation functions H_i along with the standard Jacobian of the transformation.

$$J = \begin{bmatrix} \frac{\partial y_2}{\partial r} & \frac{\partial y_3}{\partial r} \\ \frac{\partial y_2}{\partial s} & \frac{\partial y_3}{\partial s} \end{bmatrix} \tag{6}$$

Fig. 2(c) describes a typical four-sided quadrilateral cell labeled as (β). Let $\mathbf{n}^{(\beta_k)}$ denote the normal vector to side $k = 1,2,3,4$. The average displacement and traction vectors are also shown on each side. The average displacement vector $\bar{\boldsymbol{u}}^{(\beta_k)}$ on the side of the cell is defined by

$$\bar{\boldsymbol{u}}^{(\beta_k)} = \frac{1}{l_k}\int_{S_k} \boldsymbol{u}^{(\beta)}(\boldsymbol{y}) dS_k = \frac{1}{l_k}\int_{-1}^{1} \boldsymbol{u}^{(\beta)}(r,s) J_{S_k} d\xi_k = \frac{1}{2}\int_{-1}^{1} \boldsymbol{u}^{(\beta)}(r,s) d\xi_k \tag{7}$$

where l_k is the length of the side (equal to the area S_k of this side with unit thickness). The integration is defined in the physical space and performed using the parametric transformation coordinates. The line Jacobian J_{S_k} used in the present case of linear mapping has the value: $J_{S_k} = l_k/2$. In the above equation, the integration variables $d\xi_k$ assume the value dr or ds depending the specified side.

The average traction vector $\bar{\mathbf{T}}^{(\beta_k)}$ on the side of the cell is defined by

$$\bar{\boldsymbol{T}}^{(\beta_k)} = \frac{1}{l_k}\int_{S_k} \boldsymbol{\sigma}^{(\beta)}(\boldsymbol{y}) \cdot \boldsymbol{n}^{(\beta_k)} dS_k = \frac{1}{2}\int_{-1}^{1} \boldsymbol{\sigma}^{(\beta)}(r,s) \cdot \boldsymbol{n}^{(\beta_k)} d\xi_k \tag{8}$$

where $\boldsymbol{\sigma}^{(\beta)}$ is the stress field.

By substituting the quadratic form of the displacement given by Eq. (5) in Eq. (7), the average displacements on the side of the cell have the form

$$\begin{aligned} \bar{\boldsymbol{u}}^{(\beta_k)} &= \boldsymbol{u}^0 + \boldsymbol{W}^{(\beta)}_{(00)} \mp \boldsymbol{W}^{(\beta)}_{(01)} + \boldsymbol{W}^{(\beta)}_{(02)}, \quad k = 1,3 \\ \bar{\boldsymbol{u}}^{(\beta_k)} &= \boldsymbol{u}^0 + \boldsymbol{W}^{(\beta)}_{(00)} \pm \boldsymbol{W}^{(\beta)}_{(10)} + \boldsymbol{W}^{(\beta)}_{(20)}, \quad k = 2,4 \end{aligned} \tag{9}$$

where $\boldsymbol{u}^0 = \boldsymbol{\epsilon}^0 \cdot \boldsymbol{x}$ with $\boldsymbol{\epsilon}^0$ being the externally applied strain.

In order to establish the average cell side-tractions, the stresses need to be expressed in terms of the strains (constitutive equations) which in turn need to be defined using the coefficients in the displacement expansions (microvariables). The displacement gradients with respect to the physical coordinates, as functions of the parametric coordinates (r,s), are given by

$$\frac{\partial u_i}{\partial y_j}(r,s) = \frac{\partial u_i(r,s)}{\partial r}\frac{\partial r}{\partial y_j} + \frac{\partial u_i(r,s)}{\partial s}\frac{\partial s}{\partial y_j} = \hat{J}_{j1}\frac{\partial u_i(r,s)}{\partial r} + \hat{J}_{j2}\frac{\partial u_i(r,s)}{\partial s} \tag{10}$$

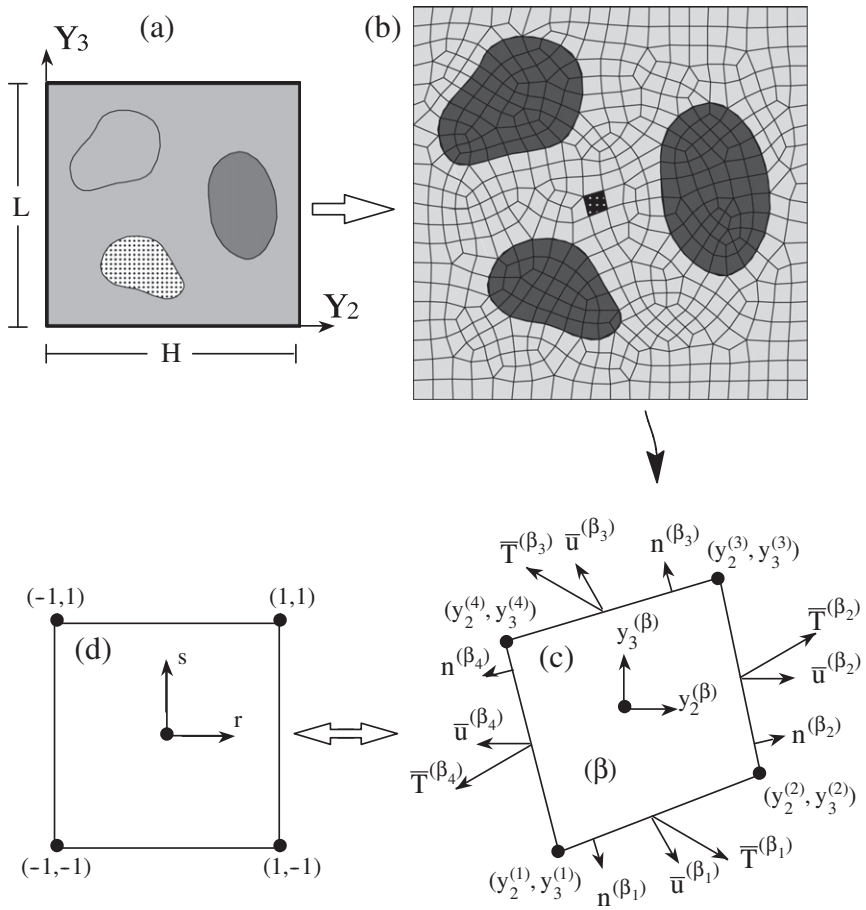

Fig. 2. (a) Schematic multiphase RUC geometry; (b) HFGMC mesh of the RUC with quadrilateral cells; (c) a representative quadrilateral cell with the normal, displacement and traction vectors shown on the four sides; (d) the mapped space of the cells.

where $\hat{J}$ is the inverse of the Jacobian that was given in Eq. (6). A direct differentiation of Eq. (5) yields

$$\frac{\partial u_i}{\partial y_j} = \hat{J}_{j1}[W_{i(10)} + W_{i(11)}s + 3W_{i(20)}r] + \hat{J}_{j2}[W_{i(01)} + W_{i(11)}r + 3W_{i(02)}s] \tag{11}$$

The spatial form of the strains in a given cell (β) are defined by

$$\epsilon_{ij}^{(\beta)}(\boldsymbol{y}(r,s)) = \epsilon_{ij}^{0} + \frac{1}{2}\left(\frac{\partial u_i}{\partial y_j} + \frac{\partial u_j}{\partial y_i}\right) \tag{12}$$

After some algebraic manipulations, the strains can be lumped in the vector form

$$\boldsymbol{\epsilon}^{(\beta)} = \boldsymbol{\epsilon}^{0} + \boldsymbol{A}^{(\beta)}\boldsymbol{W}^{(\beta)} \tag{13}$$

where the strain vector notation $\boldsymbol{\epsilon}$ is defined by

$$\boldsymbol{\epsilon}^{T} = \{\epsilon_{11}, \epsilon_{22}, \epsilon_{33}, 2\epsilon_{23}, 2\epsilon_{13}, 2\epsilon_{12}\} \tag{14}$$

The size of the vector $\boldsymbol{W}^{(\beta)}$ is 18 and includes all the microvariables of cell as follows

$$\boldsymbol{W}^{(\beta),T} = \{W_{(00)}, W_{(10)}, W_{(01)}, W_{(11)}, W_{(20)}, W_{(02)}\}^{(\beta)} \tag{15}$$

The $\boldsymbol{A}^{(\beta)}$ matrix is divided into six equal-size sub-matrices of the form

$$\boldsymbol{A}^{(\beta)} = \begin{bmatrix} \mathbf{A}_{(00)} & \mathbf{A}_{(10)} & \mathbf{A}_{(01)} & \mathbf{A}_{(11)} & \mathbf{A}_{(20)} & \mathbf{A}_{(02)} \\ 6\times 3 & 6\times 3 & 6\times 3 & 6\times 3 & 6\times 3 & 6\times 3 \end{bmatrix}^{(\beta)} \tag{16}$$

where $\mathbf{A}_{(00)}$ is a matrix of the order of 6×3 the elements of which are zeros, and

$$\boldsymbol{A}_{(10)} = \begin{bmatrix} 0 & 0 & 0 \\ 0 & \hat{J}_{(21)} & 0 \\ \hat{J}_{(11)} & 0 & 0 \\ \hat{J}_{(21)} & \hat{J}_{(11)} & 0 \\ 0 & 0 & \hat{J}_{(11)} \\ 0 & 0 & \hat{J}_{(21)} \end{bmatrix} \tag{17}$$

$$\boldsymbol{A}_{(01)} = \begin{bmatrix} 0 & 0 & 0 \\ 0 & \hat{J}_{(22)} & 0 \\ \hat{J}_{(12)} & 0 & 0 \\ \hat{J}_{(22)} & \hat{J}_{(12)} & 0 \\ 0 & 0 & \hat{J}_{(12)} \\ 0 & 0 & \hat{J}_{(22)} \end{bmatrix} \tag{18}$$

$$\boldsymbol{A}_{(11)} = s\boldsymbol{A}_{(10)} + r\boldsymbol{A}_{(01)}, \quad \boldsymbol{A}_{(20)} = 3r\boldsymbol{A}_{(10)}, \quad \boldsymbol{A}_{(02)} = 3s\boldsymbol{A}_{(10)} \tag{19}$$

Having established the spatial strains in the cell, the corresponding stresses can be obtained using the generalized Hooke's law to be employed in the expression for the average tractions, Eq. (8). This provides

$$\overline{\boldsymbol{T}}^{(\beta_k)} = \frac{1}{2}\int_{-1}^{1} \boldsymbol{N}^{(\beta_k)}\boldsymbol{C}^{(\beta)}[\boldsymbol{\epsilon}^{0} + \boldsymbol{A}^{(\beta)}\boldsymbol{W}^{(\beta)}]d\xi_k = \boldsymbol{N}^{(\beta_k)}\boldsymbol{C}^{(\beta)}[\boldsymbol{\epsilon}^{0} + \overline{\boldsymbol{A}}^{(\beta_k)}\boldsymbol{W}^{(\beta)}] \tag{20}$$

where $\boldsymbol{C}^{(\beta)}$ is the stiffness of the material in the cell and,

$$\boldsymbol{N}^{(\beta)} = \begin{bmatrix} n_1 & 0 & 0 & 0 & n_3 & n_2 \\ 0 & n_2 & 0 & n_3 & 0 & n_1 \\ 0 & 0 & n_3 & n_2 & n_1 & 0 \end{bmatrix}^{(\beta)} \tag{21}$$

and

$$\bar{\boldsymbol{A}}^{(\beta_k)} = \frac{1}{2}\int_{-1}^{1} \boldsymbol{A}^{(\beta)} d\xi_k \tag{22}$$

It should be noted that due to the applied linear mapping, the $\boldsymbol{N}^{(\beta)}$ matrix is constant.

We proceed by following the original HFGMC formulation to impose the displacements and tractions continuity between the cells along with the periodicity conditions and intra cell equilibrium. As stated above, these conditions are imposed in an average integral sense. In the following, the above transformed expressions for the average displacements and tractions, (9) and (20), respectively, can readily be used to impose the HFGMC equations. The displacements and tractions continuity can be written as

$$\bar{\boldsymbol{u}}^{(\beta_k)} = \bar{\boldsymbol{u}}^{(\gamma_m)}, \quad \overline{\boldsymbol{T}}^{(\beta_k)} = \overline{\boldsymbol{T}}^{(\gamma_m)} \tag{23}$$

where β_k denotes the kth interface (side) of cell β and γ_m is neighboring mth interface side of cell γ. The displacement and traction periodicity conditions are imposed as in Eq. (23), but with cell β and γ located on opposite sides of the RUC.

The equilibrium equations for each cell are imposed in an average sense in conjunction with Divergence theorem in order to utilize the derived expressions for the average tractions as follows

$$\int_V \nabla\cdot\boldsymbol{\sigma} dV = \int_S \boldsymbol{\sigma}\cdot\boldsymbol{n} dS = \sum_{k=1}^{4}\int_{S_k} \boldsymbol{N}^{(\beta_k)}\boldsymbol{\sigma}^{(\beta)} dS_k = \sum_{k=1}^{4} l_k \overline{\boldsymbol{T}}^{(\beta_k)} = \boldsymbol{0} \tag{24}$$

where V and S are the volume and surface of the (β)-cell, respectively, and l_k is the length of the kth side.

The total number of unknown microvariables in the RUC is $18N_c$ where N_c is the total number of cells every one of which has 18 microvariables, see Eq. (5). The number of continuity and periodicity equations for displacements is $3\times 2N_c$ (only two interfaces for each cell provide independent relations), see the first equality in Eq. (23). Similarly, the number of traction continuity and periodicity equations is $3\times 2N_c$. The average equilibrium relations, Eq. (24), provide $3N_c$ equations. Thus additional $3N_c$ equations are needed. To this end, the moment of the equilibrium equations can be used. This is expressed as follows

$$\begin{aligned}\int_V y_2 y_3 \nabla\cdot\boldsymbol{\sigma} dV &= \int_V \nabla\cdot(y_2 y_3\boldsymbol{\sigma}) dV - \int_V y_2\boldsymbol{\sigma}\cdot\hat{\boldsymbol{e}}_3 dV - \int_V y_3\boldsymbol{\sigma}\cdot\hat{\boldsymbol{e}}_2 dV \\ &= \int_S y_2 y_3\boldsymbol{\sigma}\cdot\boldsymbol{n} dS - \boldsymbol{S}_{(10)}\cdot\hat{\boldsymbol{e}}_3 - \boldsymbol{S}_{(01)}\cdot\hat{\boldsymbol{e}}_2 \\ &= \sum_{k=1}^{4}\frac{l_k}{V}\overline{\boldsymbol{T}}^{(\beta_k)}_{(11)} - \boldsymbol{S}_{(10)}\cdot\hat{\boldsymbol{e}}_3 - \boldsymbol{S}_{(01)}\cdot\hat{\boldsymbol{e}}_2 = \boldsymbol{0}\end{aligned} \tag{25}$$

where the volume average stress moments are generally defined as

$$\boldsymbol{S}_{(mn)} = \frac{1}{V}\int_V y_2^m y_3^n \boldsymbol{\sigma} dV \tag{26}$$

and

$$\overline{\boldsymbol{T}}^{(\beta_k)}_{(mn)} = \frac{1}{l_k}\int_{S_k} y_2^m y_3^n \boldsymbol{\sigma}\cdot\mathbf{n} dS_k \tag{27}$$

with $\hat{\mathbf{e}}_2$, $\hat{\mathbf{e}}_3$ being the unit vectors in the y_2 and y_3-directions, respectively.

Next, the established HFGMC $18\times N_c$ governing equations of the RUC are solved to obtain the unknown 18 microvariables for each cell. These equations can symbolically be grouped into four parts in the form

$$\begin{bmatrix} \mathbf{A}_u^{(+)} - \mathbf{A}_u^{(-)} \\ \mathbf{A}_T^{(+)} - \mathbf{A}_T^{(-)} \\ \sum \mathbf{A}_T^{(+)} - \sum \mathbf{A}_T^{(-)} \\ \sum y_1 y_2 \mathbf{A}_T^{(+)} - \sum y_1 y_2 \mathbf{A}_T^{(-)} \end{bmatrix}\{\mathbf{W}\} + \begin{bmatrix} \mathbf{0} \\ \mathbf{D}_T^{(+)} - \mathbf{D}_T^{(-)} \\ \mathbf{0} \\ \mathbf{0} \end{bmatrix}\{\boldsymbol{\epsilon}^0\} = \begin{Bmatrix} \mathbf{0} \\ \mathbf{0} \\ \mathbf{0} \\ \mathbf{0} \end{Bmatrix} \tag{28}$$

where the first part (row) represents the average continuity and periodicity of the displacements, the second part represents the continuity of the tractions in a similar fashion. The third and the fourth parts represent the equilibrium equations and their moments for all the cells. The above system of equations is solved for an externally applied strains $\boldsymbol{\epsilon}^0$ to obtain the cell microvariables. Furthermore, the local spatial strains are readily obtained using Eq. (13) which leads to the spatial distribution of the stresses in the RUC.

The set of HFGMC equation (28), is singular in its present form since the rigid-body motion has not been eliminated. To this end, it is convenient to impose a pointwise zero displacement at the mid-side points of the corner cells of the RUC. These displacement boundary conditions are expressed by appropriately setting to zero one of the following four equations:

$$\begin{aligned}\boldsymbol{u}(\pm 1, 0) &= \boldsymbol{\epsilon}^0\cdot\mathbf{x} + \mathbf{W}_{(00)} \pm \mathbf{W}_{(10)} + \mathbf{W}_{(20)} - \frac{1}{2}\mathbf{W}_{(02)} \\ \boldsymbol{u}(0, \pm 1) &= \boldsymbol{\epsilon}^0\cdot\mathbf{x} + \mathbf{W}_{(00)} \pm \mathbf{W}_{(01)} - \frac{1}{2}\mathbf{W}_{(20)} + \mathbf{W}_{(02)}\end{aligned} \tag{29}$$

The ability to apply pointwise displacement boundary conditions stems from the current HFGMC formulation whereby it is not solely based on the average deformation field of the cell. A choice of average variables in the derivation may impair the flexibility of the HFGMC implementation.

The effective elastic properties of the multiphase composite can be obtained from the cell strain concentration tensors $\boldsymbol{G}^{(\beta)}$. The latter is established by considering the average strain of the cell having the form

$$\bar{\boldsymbol{\epsilon}}^{(\beta)} = \frac{1}{V}\int_V \boldsymbol{\epsilon}(\boldsymbol{y}) dV = \boldsymbol{\epsilon}^0 + \frac{1}{2V}\int_V (\nabla_{\boldsymbol{y}}\boldsymbol{u} + \boldsymbol{u}\nabla_{\boldsymbol{y}}) dV \tag{30}$$

By using the Divergence theorem and the linear mapping, Eq. (30) takes the form

$$\begin{aligned}\bar{\boldsymbol{\epsilon}}^{(\beta)} &= \boldsymbol{\epsilon}^0 + \frac{1}{2V}\int_S (\boldsymbol{u}\otimes\boldsymbol{n} + \boldsymbol{n}\otimes\boldsymbol{u}) dS \\ &= \boldsymbol{\epsilon}^0 + \frac{1}{2V}\sum_{k=1}^{4} l_k (\bar{\boldsymbol{u}}\otimes\boldsymbol{n} + \boldsymbol{n}\otimes\bar{\boldsymbol{u}})^{(\beta_k)} \equiv \boldsymbol{G}^{(\beta)} : \boldsymbol{\epsilon}^0\end{aligned} \tag{31}$$

As can be observed from the Eq. (31), the concentration tensor $\boldsymbol{G}^{(\beta)}$ depends on the average displacement vectors on the surfaces of the cell. Those can be computed only after solving the entire HFGMC system of equations for the RUC. Once the concentration tensors $\boldsymbol{G}^{(\beta)}$ have been obtained, the effective elastic stiffness tensor $\boldsymbol{C}^*$ is evaluated from

$$\boldsymbol{C}^* = \sum_{\beta=1}^{N_c} v_\beta \boldsymbol{C}^{(\beta)}\boldsymbol{G}^{(\beta)} \tag{32}$$

where $v_\beta = V/V_{\mathrm{RUC}}$, and $V_{\mathrm{RUC}} = H\,L$ being the volume of the RUC.

3. Damage formulation

Damage in composite materials is of a local and distributed nature due to multi-site imperfections, such as voids and micro-cracking in the matrix phase. Damage characteristics include

multi-mode and anisotropic, initial benign states, and slow to sudden evolution rates. These offer a formidable challenge in the mechanics of damage in composite materials, especially if the goal is to describe both local and macro-behavior at all stages of the material life span. This is an active and wide area of research and over the last two decades has seen major advances. Several early landmark publications have made continuum damage mechanics a classical subject and an independent area in mechanics, e.g., Kachanov (1986), Mura (1987), Lemaitre and Chaboche (1990), Krajcinovic (1996), Lemaitre (1996), Voyiadjis and Kattan (2005) and Lemaitre and Desmorat (2005) among many others. However, there are many challenges that make damage mechanics a current and an active area of research especially in composite materials.

Damage in polymeric and metal matrix composites have been the subject of numerous studies. The wide range of damage modes that are present in the composite material, e.g., delamination, matrix cracking, fiber microbuckling, etc., justify their independent study. This makes it difficult, if not impossible, to model damage in a unified manner. Examples of such investigations are Allen et al. (1994), Boyd et al. (1993), Chow and Lu (1989), Majumdar et al. (1993), Matzenmiller et al. (1995), Talreja (1985a,b), Talreja (1994), Voyiadjis (1993), Voyiadjis and Allen (1996), Voyiadjis and Kattan (1999) and references cited there.

The use of coupled three-dimensional micromechanics with damage in the constituents offer an advantage mainly that the effective damaged response evolves naturally from the formulation without a priory assumption over its anisotropic nature and progression. Haj-Ali and Aboudi (2009) introduced progressive damage in polymeric composites in conjunction with GMC re-formulation to allow for softening damage behavior. Voyiadjis and Deliktas (1997) have introduced anisotropic damage formulation with the GMC micromechanics for the analysis of metal matrix composites. Bednarcyk et al. (2010) employed the HFGMC to include multiaxial progressive damage in the elastic matrix constituents.

Micromechanical and damage formulation can be coupled with multiscale analysis of composite materials and structures, e.g., Haj-Ali et al. (2006), Haj-Ali (2008, 2009). However, the refined micromechanical prediction of the HFGMC can offer a great advantage if coupled with damage. This is because local damaged response can be attained along with the effective softening. In this section, the proposed HFGMC micromechanical formulation is modified to implement progressive damage at the microlevel within the constituents. The key idea herein is to apply a damage criterion and the resulting softening effects at the cell level. In this way both micromechanical and damage analyses are coupled without the need to be a priori specified and thus constrain the effective damage response of the composite. The proposed ability to couple micromechanics-damage formulation offers great advantage among which the effective damage evolution emerges naturally and need not to be assumed. To this end, two major damage approaches are considered. The first is termed *cell extinction damage* (CED) approach where cells in HFGMC are degraded and then removed from the RUC model by appropriately modifying the governing micromechanical equation developed in the previous section. The second micromechanical damage approach, is based on the application of cohesive interfacial models for each cell. Here, the displacement continuity equations for the undamaged state are modified to include discontinuities expressed in terms of the interfacial tractions at the onset of damage. The latter tractions are multiplied by selected interfacial compliance functions. However, it is important to note the limitation of introducing damage within the RUC micromechanical formulation. This is because the periodicity conditions in the latter formulation are also imposed on the damage initiation and evolution in the entire composite material. As a result, the predicted damage formations are limited in the sense that they are not independent in the inter-RUCs. In order to address the practical need for damage modeling in composite structures, the proposed periodic damage formulation should be implemented in a multiscale analysis framework and applied at a relatively large number of spatial locations.

In the framework of the first CED damage approach, damage initiation in the cell is governed by a stress or strain-based criterion, such the Mises equivalent stress function for the isotropic matrix cells, e.g., Lemaitre and Chaboche (1990). Once damage initiates, a strain softening scheme is applied in the cell whereby the stiffness of the cell is degraded. Here, an isotropic damage model can be adopted for simplicity as follows

$$\boldsymbol{\sigma}^{(\beta)} = (1-\lambda^{(\beta)})\mathbf{C}^{(\beta)} : \boldsymbol{\epsilon}^{(\beta)} \tag{33}$$

where $0 \leqslant \lambda^{(\beta)} \leqslant 1$ is the associated damage variable and $\mathbf{C}^{(\beta)}$ is the stiffness of the β-cell, respectively. For simplicity, a linear relation between the cell damage variable and the equivalent strain $\epsilon_{eq}^{(\beta)}$ of the cell is adopted in the form

$$\lambda = \frac{1}{1-\eta}\left[1-\frac{\epsilon_{eq}}{\epsilon_i}\right]; \quad \epsilon_f = \eta\epsilon_i \tag{34}$$

where $\epsilon_{eq} = \epsilon_i$ is the strain condition at damage initiation and $\epsilon_{eq} = \epsilon_f$ is the strain level at which the cell is removed. The parameter η can be used to relate the initiation of damage to the final state where the cell is removed. Its limit values ($\eta = 1, \infty$) correspond to highly brittle and highly ductile (perfectly plastic) states, respectively. A loading state is defined by

$$\dot{\lambda} \geqslant 0 \quad \text{when } \epsilon_{eq} = \epsilon_{max} \quad \text{and} \quad \dot{\epsilon}_{eq} \geqslant 0 \tag{35}$$

A state of unloading or re-loading after unloading is defined by

$$\dot{\lambda} = 0 \quad \text{and} \quad \lambda = \lambda_{max} \quad \text{when } \epsilon_{eq} \leqslant \epsilon_{max} \text{ or } \dot{\epsilon}_{eq} < 0 \tag{36}$$

This simple damage evolution has been adopted in the present study. However, the proposed micromechanics-damage framework is quite general and other damage evolution laws can be easily implemented. The current damage formation has been carried out with isotropic (scalar) damage variables associated with each subcell in the RUC. However, this is not a limitation and tensorial damage variables can be easily introduced in each subcell.

At a pre-selected damage level, $\lambda^{(\beta)} = \lambda_f$ the cell is removed from the model thus creating a traction-free surfaces. This is achieved in the present HFGMC formulation by eliminating the displacement continuity equations of the four sides of the cell, the first part of Eq. (23). In addition, the traction continuity equations, the second part of Eq. (23), are replaced by setting Eq. (20) to zero for the adjacent cells. Furthermore, the equilibrium equations, (24) and (25), are also removed from the overall system of equation, (28). As a result, the system of equations has been reduced by 18 variables and equations. This procedure creates imbalance in the overall HFGMC system of equations and a load redistribution is needed. Therefore, an iterative predictor–corrector procedure must be implemented in order to reach the correct displacement microvariables and the associated consistent damage variables in the cells. The iterative solution procedure requires the definition of a cell residual vector defined by

$$\boldsymbol{R}^{(\beta)} = \left\{ \begin{array}{c} \bar{\boldsymbol{u}}^{(\beta_k)} - \bar{\boldsymbol{u}}^{(\gamma_m)} \\ \bar{\boldsymbol{T}}^{(\beta_k)} - \bar{\boldsymbol{T}}^{(\gamma_m)} \\ \int_V \nabla \cdot \boldsymbol{\sigma} dV \\ \int_V y_2 y_3 \nabla \cdot \boldsymbol{\sigma} dV \end{array} \right\}; \quad \mathbf{R}^{(\beta)} \to \mathbf{R}_G \tag{37}$$

The global residual vector, $\boldsymbol{R}_G$, is established by collecting the individual residual vectors of the cells. The latter are evaluated by a numerical integration over the surface and volumes of the cells. The linearization of the global residual vector results in the system

of equations which has been previously established in Eq. (28). By equating the residual vector $\boldsymbol{R}_G$ to the residual form of Eq. (28) it is possible to apply linearization to both sides and establish an incremental solution procedure. This can be represented by

$$\boldsymbol{R}_G = \boldsymbol{A}\boldsymbol{W} - \boldsymbol{D}\boldsymbol{\epsilon}^0 = \boldsymbol{0} \tag{38}$$

Therefore

$$\Delta \boldsymbol{W} = -\left[\frac{\partial \boldsymbol{R}_G}{\partial \boldsymbol{W}}\right]^{-1}_{\lambda,\boldsymbol{W}} = -\boldsymbol{A}^{-1}\boldsymbol{R}_G \tag{39}$$

where the $\boldsymbol{A}$-matrix is evaluated at a fixed damage and microvariables from the previous time step $t - \Delta t$. With the established global residual vector and its linearized form, it is possible to proceed with an incremental iterative procedure aimed at satisfying the overall HFGMC equations in their total form while consistently updating the deformation field and damage variables.

The algorithmic solution procedure is summarized in Fig. 3. The described algorithm begins with a given prior converge solution state at time $t - \Delta t$ along with the material and damage history variables His_m and $\lambda^{(\beta)}$ in the cell. A trial elastic solution update is first generated for an applied $\boldsymbol{\epsilon}^0$ using the system of equations (28) in conjunction with the previously computed $\boldsymbol{A}$ and $\boldsymbol{B}$ matrices. Steps 4 and 5 in the solution algorithm, Fig. 3, describe two nested iterative loops, the first of which damage iteration updates are conducted, whereas the second one incremental iterative procedure is carried out to generate a converge solution for the microvariables. The previously described global residual vector (37) is evaluated during both nested loops following the updates over the damage and microvariables, respectively. A convergence is reached once the two residual checks are satisfied as shown in steps 5.3 and 6.1 in Fig. 3.

In the cohesive micromechanical-damage modeling can be implemented by modifying the displacements interfacial continuity conditions, the first part of Eq. (23), to

$$[\bar{\boldsymbol{u}}]^{(\beta_k\gamma_m)} - \boldsymbol{\Omega}^{(\beta_k\gamma_m)}\overline{\boldsymbol{T}}^{(\beta_k)} = \bar{\boldsymbol{u}}^{(\beta_k)} - \bar{\boldsymbol{u}}^{(\gamma_m)} - \boldsymbol{\Omega}^{(\beta_k\gamma_m)}\overline{\boldsymbol{T}}^{(\beta_k)} = \boldsymbol{0} \tag{40}$$

where $[\bar{\boldsymbol{u}}]$ denotes the average displacement jump across the interface between the kth-side of cell (β) and the mth-side of the neighboring cell (γ). The interfacial compliance matrix $\boldsymbol{\Omega}^{(\beta_k\gamma_m)}$ between these adjacent cell sides of the interface can depend on the displacement jump $[\bar{\boldsymbol{u}}]$. In this case, it is possible to associate damage variables with the cohesive interface, in the same manner as was previously given in the CED formulation. To this end, the interfacial traction can be expressed by

1. Input variables: ε^o ; Δt

Recall prior converged solution state: $\overline{\varepsilon}^{t-\Delta t}$; $\overline{\sigma}^{t-\Delta t}$; $\text{Hist}^{t-\Delta t}$: $\{W,\ \sigma,\ \text{Hist\_m},\ \lambda\}^{(\beta),t-\Delta t}$

2. Initialize linearized equations using prior damage state

$W^{(\beta),t-\Delta t} \rightarrow \varepsilon^{(\beta),t-\Delta t}$; $\text{Hist}^{(\beta);\,t-\Delta t} \rightarrow C^{(\beta),\,t-\Delta t}$ Eq. (13)

3. Perform trial elastic update and solve assemble overall system:

$A^{t-\Delta t}\ W^t = D^{t-\Delta t}\ \varepsilon^o$

$W^{(\beta),t} \rightarrow W^{(\beta),i=0}$; $\Delta W^{(\beta),i=0} = 0$ Eq. (28)

4. Damage iterative update for k=1, 2, 3....

5. Iterative solution for i=1, 2, 3....

5.1 Evaluate trial microvariables: $\sigma^{(\beta\gamma),t}$; $\text{Hist}^{(\beta\gamma),t}$; $C^{(\beta\gamma),t}$

$W^{(\beta),i-1} + \Delta W^{(\beta),i} \rightarrow W^{(\beta),i}$

$W^{(\beta),i} \rightarrow \varepsilon^{(\beta),i}$

5.2 Perform total constitutive stress updates for all cells

$\sigma^{(\beta),i}$; $\text{Hist}^{(\beta),i}$; $C^{(\beta),i}$

5.3 Assemble residual error vector: $R^{(\beta),t} \rightarrow R^i_G$ Eq. (37) and Eq. (40)

IF $\| R^i_G \| \le \text{Tol}$ THEN GOTO 6

ELSE

5.4 Compute the correction for the microvariables:

$$\Delta W^i \equiv W^i - W^{i-1} = -\left[\frac{\partial R^i_G}{\partial W^i}\right]^{-1}_{i-1} R^i_G = \left[A^{t,\,i-1}\right]^{-1} R^i_G \quad \text{Eq. (39)}$$

$\Delta W^i \rightarrow \Delta W^{(\beta),i}$

REJECT: $\sigma^{(\beta),i}$; $\text{Hist}^{(\beta),i}$; $C^{(\beta),i}$, Assemble $A^{t,i}$ and GOTO 5

ENDIF

6. Update damage variables, $\lambda^{(\beta)}$, stresses, and overall stiffness:

6.1 Assemble residual error vector: $R^{(\beta),i} \rightarrow R^k_G$

IF $\| R^k_{\text{HFGMC}} \| \le \text{Tol}$ THEN GOTO 7

ELSE GOTO 4

ENDIF

7. Update local microvariables, stresses, overall effective tangent stiffness:

$W^{(\beta),i} \rightarrow W^{(\beta),t}$; Hist^t : $\{W,\ \sigma,\ \text{Hist\_m},\ \lambda\}^{(\beta),t}$; C^* ; $\overline{\sigma}$

EXIT

Fig. 3. Iterative solution algorithm for the HFGMC micromechanical-damage method illustrating an incremental and total formulation along with state variable updates.

$$\overline{\boldsymbol{T}}^{(\beta_k)} = \left[\boldsymbol{\Omega}^{(\beta_k\gamma_m)}\right]^{-1}[\overline{\boldsymbol{u}}]^{(\beta_k\gamma_m)} \equiv (\boldsymbol{I}-\boldsymbol{\lambda})\boldsymbol{C}_0[\overline{\boldsymbol{u}}]^{(\beta_k\gamma_m)} \tag{41}$$

where $\boldsymbol{C}_0$ is the initial interfacial stiffness which is subsequently degraded by the damage matrix $\boldsymbol{\lambda}$. This equation relates the interfacial compliance tensor to the current interface stiffness through its initial value and the cohesive damage variables. The loading and loading conditions in this cohesive damage model can be defined in a similar manner to those in the CED model, Eqs. (35) and (36).

Alternatively, $\boldsymbol{\Omega}^{(\beta_k\gamma_m)}$ can have a fixed value to represent a pre-existing state of interfacial damage. Another possibility is to assume an increasing time dependent function whereby the debonding history is prescribed a priori $\boldsymbol{\Omega}^{(\beta_k\gamma_m)}(t)$, Bednarcyk and Arnold (2002) and Bednarcyk et al. (2004). Finally, it is important to note that in this cohesive damage modeling the traction continuity conditions remain intact. The creation of free traction surfaces is automatically carried out in the limit $\boldsymbol{\Omega}^{(\beta_k\gamma_m)} \to \infty$.

The interfacial compliance matrix $\boldsymbol{\Omega}^{(\beta_k\gamma_m)}$ defined in Eq. (40) is written in the global RUC coordinate system. It is possible to rewrite this equation in the local interface coordinate system, having the base unit vectors $(\hat{\boldsymbol{e}}_1, \hat{\boldsymbol{e}}_n, \hat{\boldsymbol{e}}_t)$, as:

$$[\overline{\boldsymbol{u}}]'^{(\beta_k\gamma_m)} - \boldsymbol{\Omega}'^{(\beta_k\gamma_m)}\overline{\boldsymbol{T}}'^{(\beta_k)} = \boldsymbol{0} \tag{42}$$

where

$$[\overline{\boldsymbol{u}}]'^{(\beta_k\gamma_m)} = \boldsymbol{a}[\overline{\boldsymbol{u}}]^{(\beta_k\gamma_m)}, \quad [\overline{\boldsymbol{T}}]'^{(\beta_k\gamma_m)} = \boldsymbol{a}[\overline{\boldsymbol{T}}]^{(\beta_k\gamma_m)},$$
$$\boldsymbol{\Omega}^{(\beta_k\gamma_m)} = \boldsymbol{a}^T\boldsymbol{\Omega}'^{(\beta_k\gamma_m)}\boldsymbol{a} \tag{43}$$

with $\boldsymbol{a}$ being the standard vector transformation matrix. The resulting transformation shown above yields the $\boldsymbol{\Omega}^{(\beta_k\gamma_m)}$: the interfacial compliance matrix in the (Y_2, Y_3) coordinates of the RUC. The local interfacial compliance matrix $\boldsymbol{\Omega}'(\beta_k\gamma_m)$ has the following diagonal form:

$$\boldsymbol{\Omega}'^{(\beta_k\gamma_m)} = \begin{bmatrix} \Omega'_{11} & 0 & 0 \\ 0 & \Omega'_{nn} & 0 \\ 0 & 0 & \Omega'_{tt} \end{bmatrix}^{(\beta_k\gamma_m)} \tag{44}$$

The implementation of the cohesive micromechanics-damage model requires the solution of a nonlinear set of equations in the case where interfacial compliance matrix is dependent on the displacement. This necessitates an iterative solution procedure with similar considerations as stated above in the CED approach. However, the residual vector in the present case is of the form

$$\boldsymbol{R}^{(\beta)} = \begin{Bmatrix} \overline{\boldsymbol{u}}^{(\beta_k)} - \overline{\boldsymbol{u}}^{(\gamma_m)} - \boldsymbol{\Omega}^{(\beta_k\gamma_m)}\overline{\boldsymbol{T}}^{(\beta_k)} \\ \overline{\boldsymbol{T}}^{(\beta_k)} - \overline{\boldsymbol{T}}^{(\gamma_m)} \\ \int_V \nabla\cdot\boldsymbol{\sigma}dV \\ \int_V y_2 y_3 \nabla\cdot\boldsymbol{\sigma}dV \end{Bmatrix} \tag{45}$$

4. Applications

The application section is divided into two major parts. The first deals with the verifications of the proposed HFGMC theory with linear mapping. To this end, RUC models are generated and comparisons with analytical and numerical solutions are presented to demonstrate the ability of the HFGMC to capture the spatial stress field distributions within the phases. These applications illustrate the new capability to predict the elastic field in the phases with general geometry. Special effort has been given to generate RUCs with moderate or even small number of cells in order to demonstrate the additional computational efficiency of the new derivation. The second part of this section presents progressive damage applications where the current HFGMC formulation is extended to include evolving and strain softening damage using the CED method.

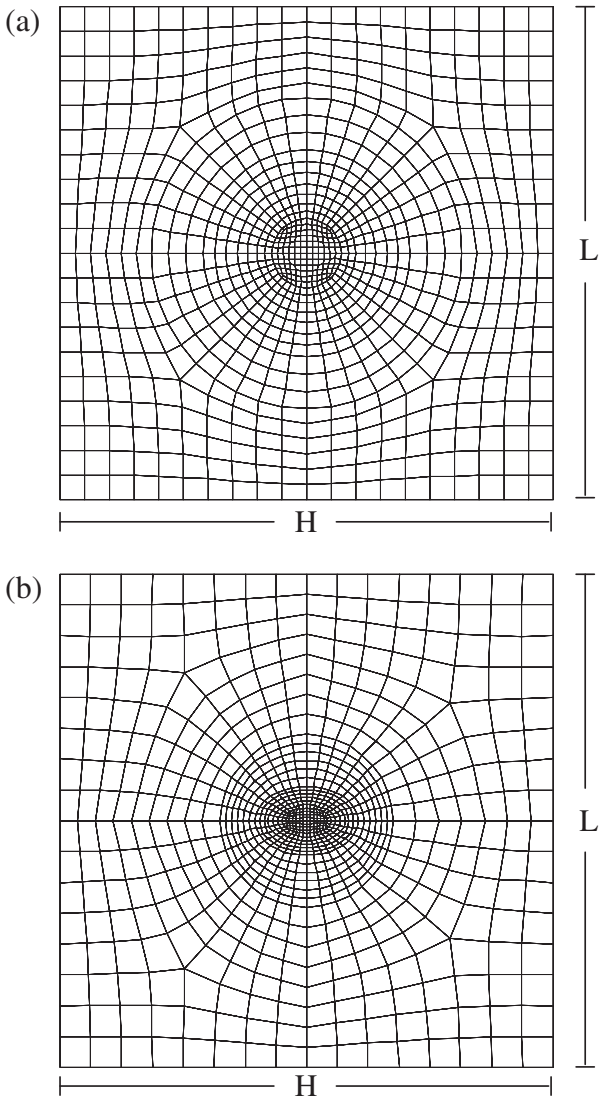

Fig. 4. HFGMC meshes for two RUCs; (a) square array with a circular fiber; (b) square array with an elliptical fiber.

Consider two diluted unidirectional composite systems whereby fibers with circular and elliptical cross-sections are oriented in the *1*-direction. Fig. 4(a) and (b) shows the HFGMC cell meshes for the RUCs of these two composites. The number of quadrilateral cells used in these two RUC models are: 880 and 524, respectively, and both RUCs share the same dimensions, $H = L$. In the first RUC, the ratio of the radius of the circular fiber to H is 0.1. As for the second RUC with elliptical fiber, the ratio of the major and minor radii to H are: 0.05 and 0.025, respectively. The material for the fibers is taken as glass with Young's modulus and Poisson's ratio of $E = 69$ GPa and $\nu = 0.2$, respectively. The matrix material is epoxy with elastic constants: $E = 4.8$ GPa and $\nu = 0.34$. The composite with the circular fibers is subjected to a remote stress $\sigma_{33} = 10$ MPa together with the conditions that the effective axial strain $\bar{\epsilon}_{11} = 0$ and $\sigma_{22} = 0$. The closed-form Eshelby solution (Muskhelishvili, 1963) can be employed to verify the spatial stress distribution as predicted by the HFGMC model. Fig. 5(a)–(c) shows the HFGMC plots for the two transverse stress components σ_{22} and σ_{33} along with the transverse shear stress σ_{23}. The corresponding analytical solution plots are shown in Fig. 5(d)–(f). It can be readily observed that excellent agreement exists between the two solutions. It should be noted that a relatively small number

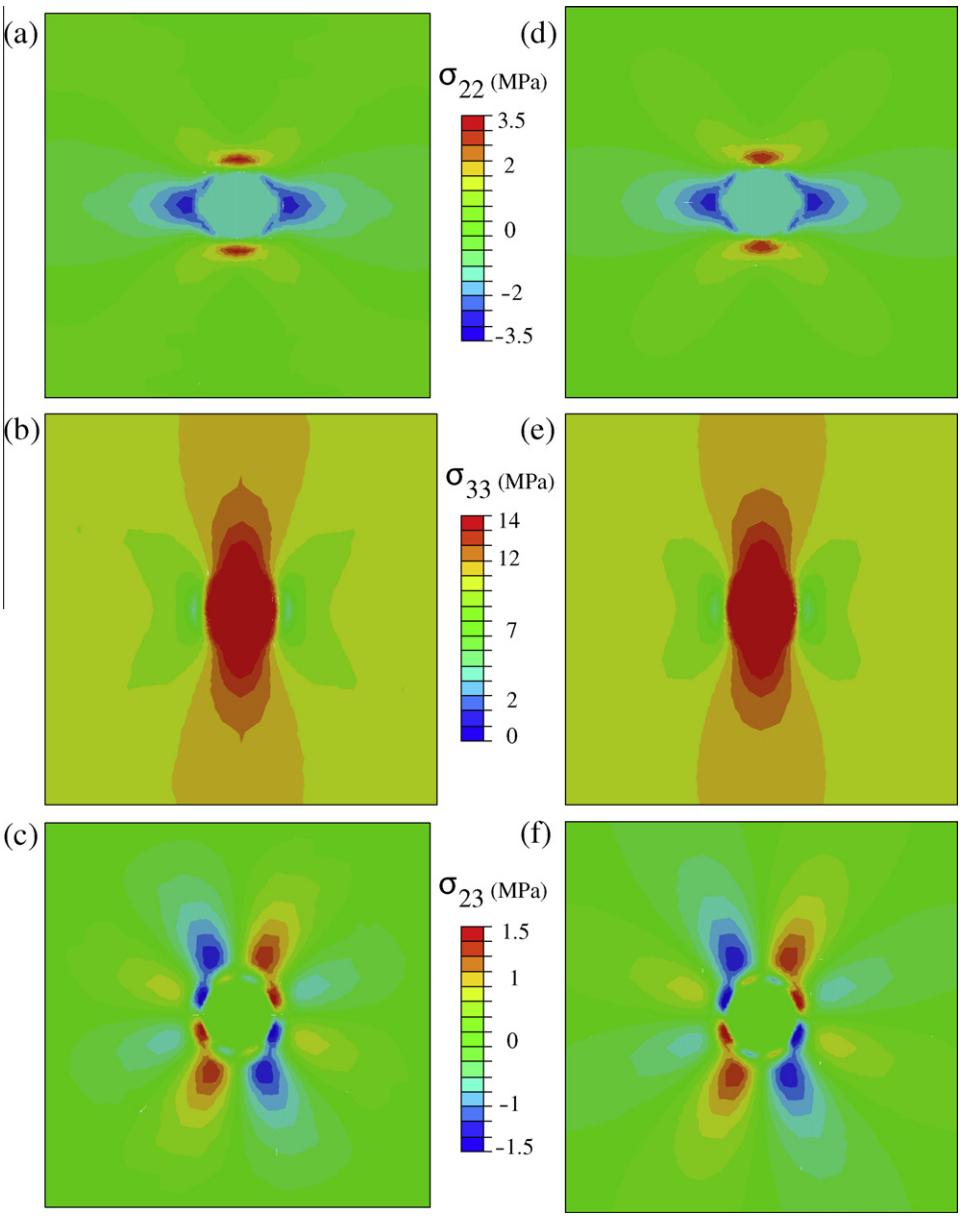

Fig. 5. Stress distributions in the RUC with circular fiber – a comparison between the HFGMC and closed-form Eshelby solutions.

quadrilateral cells has been used to generate the HFGMC solution with linear geometric mapping.

The HFGMC results for the diluted composite with elliptical cross-sectional fibers are shown in Fig. 6(a)–(d). These are compared with a finite-element (FE) solution, Fig. 6(e)–(h), having generalized plane strain elements. The number of elements in the FE solution is equal to the number of cells used in generating the HFGMC results. Fig. 6 exhibits the three normal stress distributions together with the transverse shear for both solutions. Again, it can be observed that excellent agreement exists between the two methods of solution.

Next, we proceed with applications of progressive damage using the proposed CED method implemented within the HFGMC. Towards this goal, a unidirectional composite with a fiber volume fraction $v_f = 0.385$ is considered. It is subjected to a remote uniaxial transverse strain loading of ϵ^0_{33}. A boron/epoxy material system is selected in this case where the epoxy properties are the same as those used previously and the boron elastic properties are: $E = 379.3$ GPa, $\nu = 0.1$. The HFGMC micromechanics with the CED damage method is employed to generate both the macroscopic response and local stress distributions at different levels of loading. Two types of RUCs have been considered for this composite, namely square and hexagonal packing arrays. Fig. 7(a) and (b) shows the HFGMC meshes of the RUCs for these two cases. A Mises stress criterion for the damage initiation in the interior matrix cells is applied in the form: $\sigma_{eq} = 10$ MPa. Damage is not considered for both the fiber and boundary cells in order not to violate the periodicity equations. Once damage initiation is detected, a softening procedure takes place whereby the stiffness of the cell is degraded, see Eq. (33). This cell is extinct and removed from the system of equations at a given critical value of its damage variable, $\lambda = \lambda_{crit} = 0.8$ in this case. Fig. 8 shows the effective stress–strain response of the two types of RUCs exhibiting identical initial response. It is interesting to observe that the predicted ultimate stress level for the composite with the hexagonal array distribution is somewhat higher than the corresponding stress of the square array packing. However, the strains at the ultimate stress levels coincide in the two cases. Furthermore, post ultimate progressive

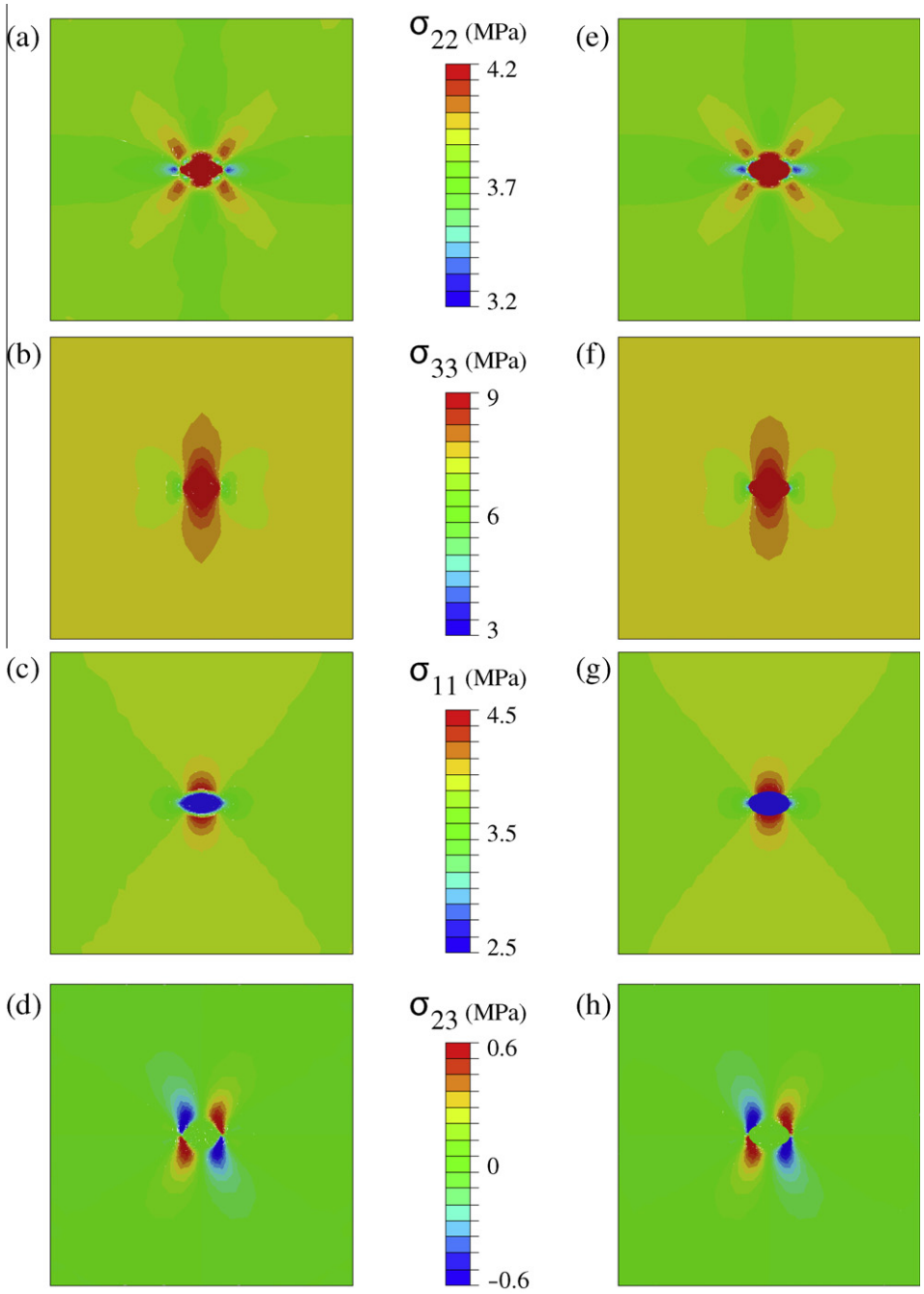

Fig. 6. Stress distributions in the RUC with an elliptical fiber – a comparison between the HFGMC and the FE solutions.

damage and energy dissipation are more rapid in the hexagonal array that of the square one. Finally, the two macroscopic stress–strain curves exhibit a re-loading after post ultimate response as evident by the positive slopes of these two curves. This is an artifact because damage was not considered in the boundary matrix cells which allow a continued loading in these cells. A damage formulation that includes the RUC periodic boundaries is a subject for further research. The spatial distributions of the local equivalent stress σ_{eq} in the square and hexagonal arrays are shown at different loading levels in Figs. 9 and 10, respectively. These sequence of stress distribution plots are chosen to illustrate the damage progression with increasing remote loading. It is interesting to observe a different progression sequence of damage in both cases. As mentioned above, fiber cells are not affected by damage and their extinction is not carried out. Nevertheless, unloading of the stress in the fiber cells is observed due to the loss of connectivity between the fiber–matrix and the creation of voided zones. It is worth mentioning that damage initiation in a cell can occur while the global stress–stain response of the composite seems not to be affected. This observation can be seen in Figs. 9(b) and 10(c) where some stress reduction zones have taken place, yet no noticeable slope change is evident in the global response. This behavior is consistent with experimental observation in the transverse tensile loading case of composites, especially when acoustic emission is used to detect early stages of damage initiations.

Finally, the interfacial cohesive damage modeling approach is utilized to investigate the previous case of square fiber array subjected to the same remote uniaxial strain loading ϵ^0_{33}. The cohesive

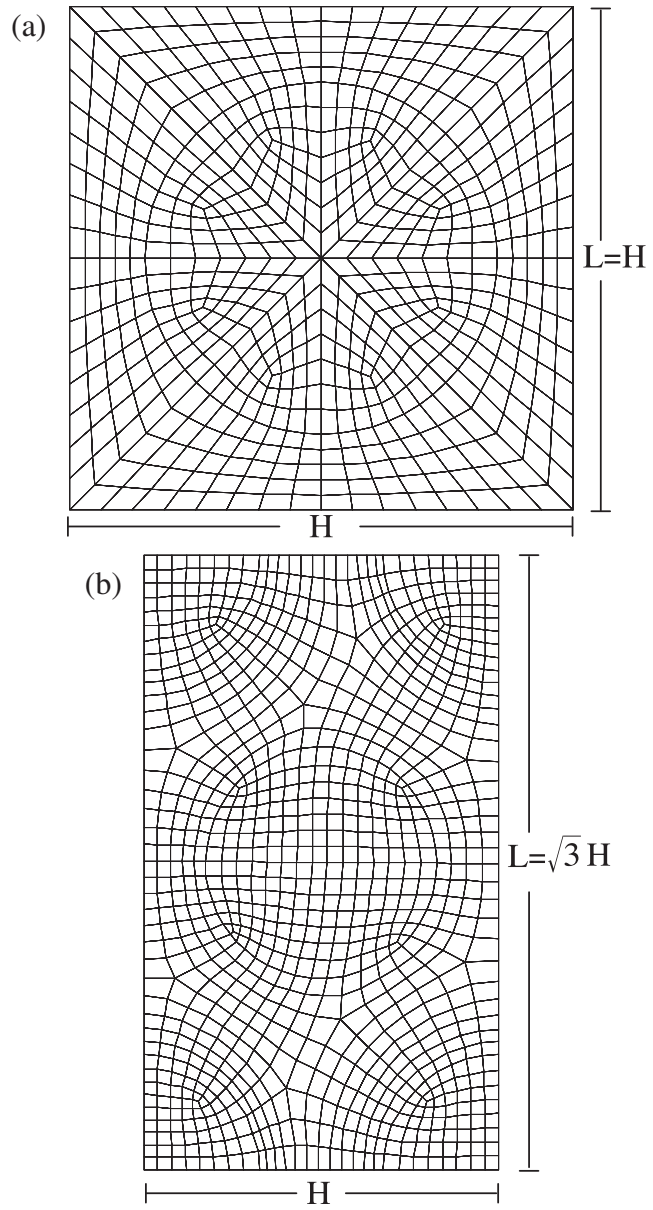

Fig. 7. HFGMC: two RUC meshes for a unidirectional composite with circular fibers: (a) square array; (b) hexagonal array.

model is implemented at the interfaces between the fiber and matrix cells. The interfacial damage initiation criterion used is the equivalent traction as proposed by Camacho and Ortiz (1996): $\overline{T}_{eq} = \sqrt{\overline{T}_n^2 + \beta_{ns}\overline{T}_s^2} > \overline{T}_{eq}^0$, where $\overline{T}_n$ and $\overline{T}_s$ are local interfacial normal and shear traction components, respectively. The term β_{ns} denotes a mixed normal-shear coupling coefficient. The properties used for the cohesive interface are: $\overline{T}_{eq}^0 = 27$ MPa, $\beta_{ns} = 0.2$. Once interfacial damage has been detected, the interfacial compliance matrix assumes a linear evolving form with time, measured from the initiation point, reaching a maximum value (full debonding) at time: $t_f = \beta_f t_i$. Here, the coefficient, β_f, relates the time at full debonding to that of initiation, its chosen value is $\beta_f = 1.05$. Fig. 11 shows the equivalent transverse stress–strain response of the boron/epoxy composite with strain softening due to the fiber–matrix interfacial damage modeled by the cohesive damage approach. Also shown in this figure, the corresponding damage behaviors of the same composite as previously modeled by the CED approach. It should be noted that the cohesive properties are calibrated to

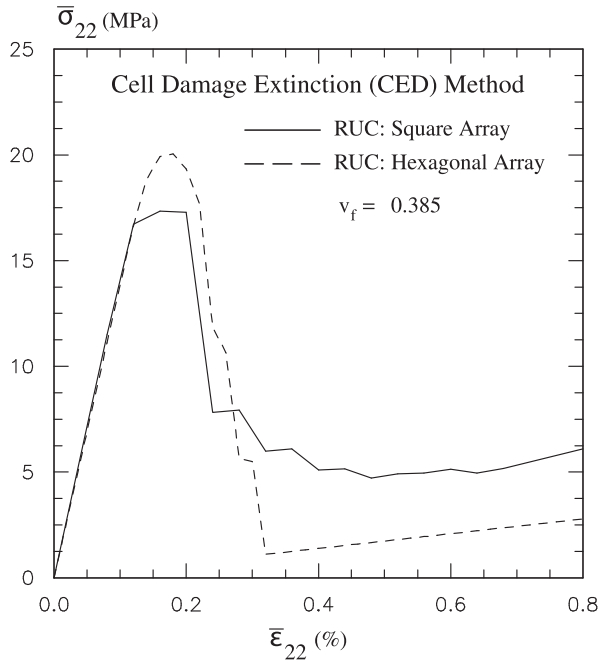

Fig. 8. Effective transverse stress–strain responses as predicted by the HFGMC with cell damage extinction method illustrating softening due to progressive damage behavior.

achieve similar effective stress–strain curves of the previous two cases. It can be observed that similar global softening takes place in both damage approaches while the cohesive model seems to be more dissipative in the post-peak response. The predicted HFGMC local stress distributions are shown in Fig. 12 with evolving damage at selected loading stages. It is interesting to observe similar initiation in the current model, Fig. 12(b), as previously shown in the CED results. However, the damage progression and fiber unloading is somewhat different.

5. Discussion

The aim of the first part of this section is to draw distinctions between the well-known displacement-based finite-element (FE) and the HFGMC methods, where a common misconception is to link the HFGMC to FE. This is not in any way to claim that the HFGMC can replace the general purpose and well-established FE method, rather to point out that the two methods are not related. In the FE formulation the displacement continuity between two adjacent and connected elements is satisfied in a pointwise manner by sharing the same nodal degrees of freedom at the sides of an element. However, the displacement continuity in the HFGMC is satisfied in an average sense between adjacent cells. The latter is an approximation that allows the HFGMC to explicitly use additional stress variables in the formulation and directly apply traction continuity in an average basis between cells. Another major difference between the two methods lies in the fact that the continuum equilibrium equations in the HFGMC are explicitly applied in a volumetric average for each cell, which allows retaining the cell stresses and their higher order moments in the formulation. In difference, the FE method employs equilibrium through the well-known virtual work or weak flux form, expressed externally using the nodal forces. The FE is a general method and can be employed to generate micromechanical models for a priori given states of applied remote fields. This typically requires the application of special numerical schemes needed to impose the proper remote traction and displacement boundary conditions in order to

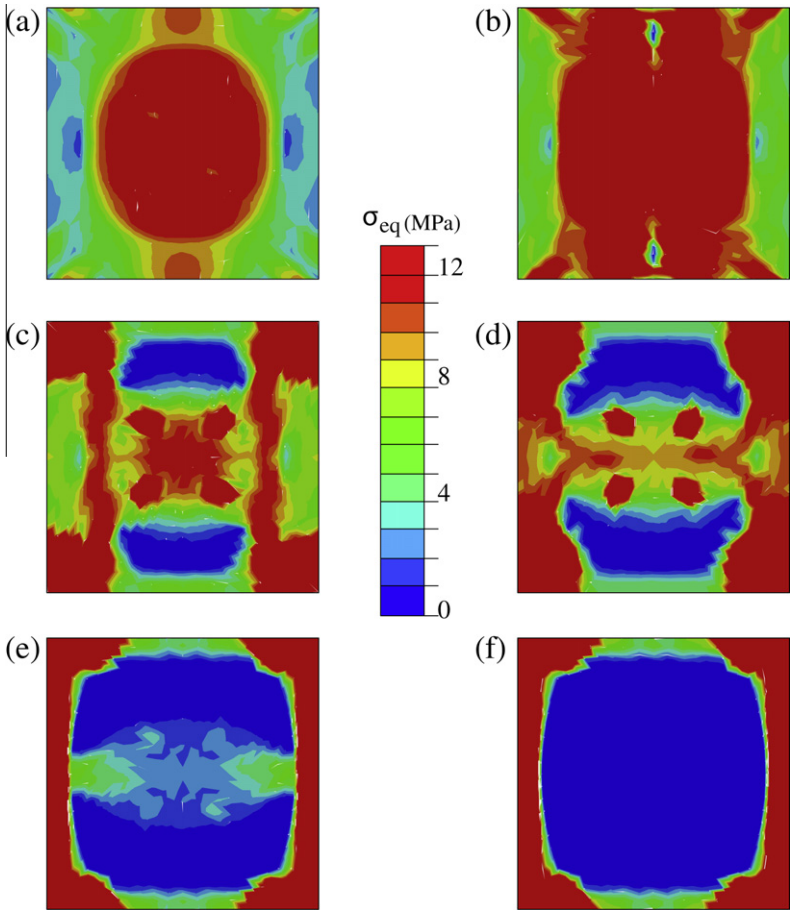

Fig. 9. Equivalent stress distribution sequence in the composite with the square array as predicted by the HFGMC with the CED evolving damage.

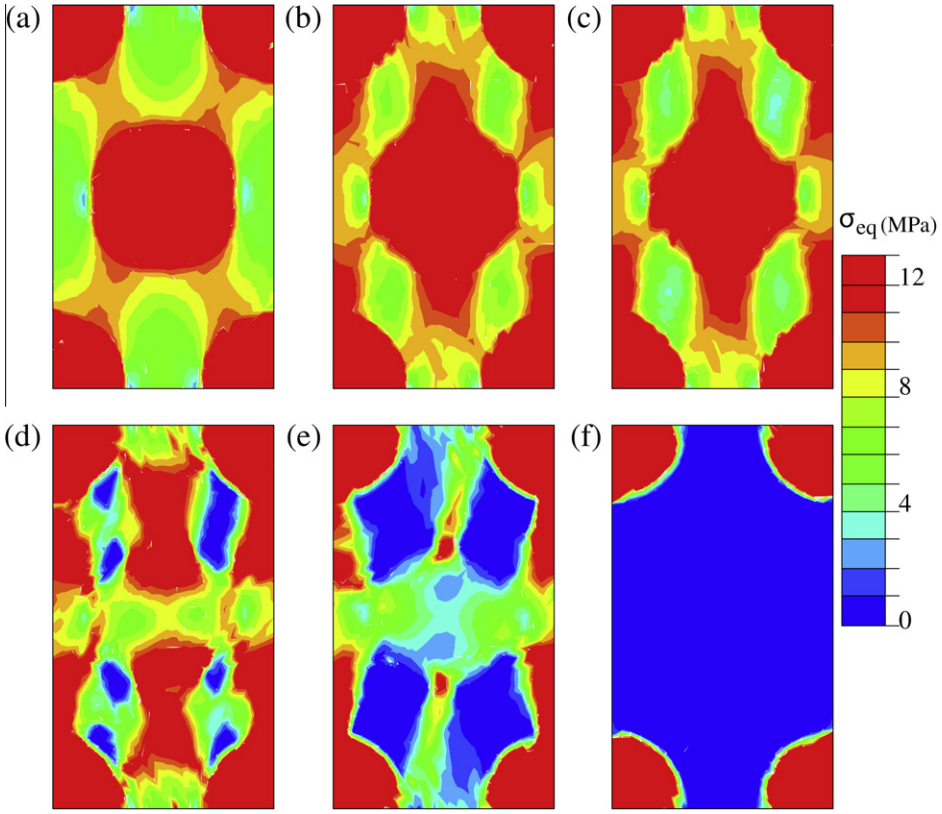

Fig. 10. Equivalent stress distribution sequence in the composite with the hexagonal array as predicted by the HFGMC with the CED evolving damage.

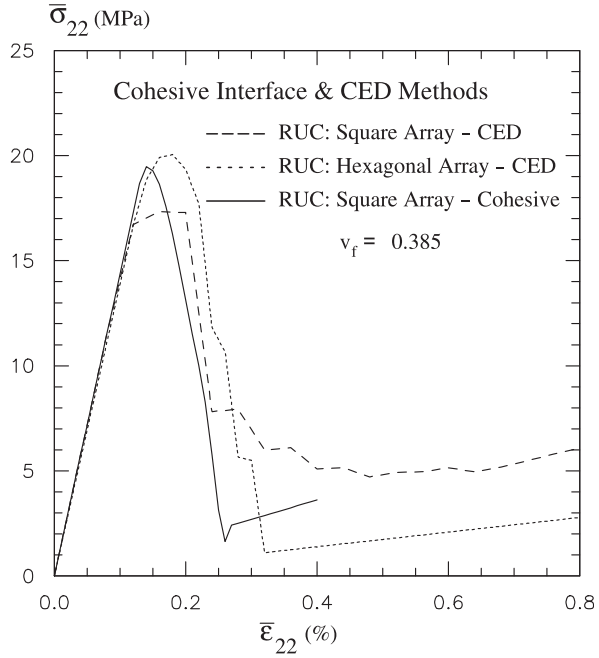

Fig. 11. Comparison between the effective transverse stress–strain responses as predicted by the HFGMC with the cell damage extinction method (CED) and the cohesive fiber–matrix interface approach.

generate the correct internal fields. Unlike FE, the HFGMC is a specialized modeling framework in which the remote fields are directly tied to the micromechanical formulation (e.g., the remote average strain is directly used in the HFGMC formulation). Finally, the periodicity in the FE formulation is imposed only through displacement boundary conditions, while in the HFGMC, the periodic boundary conditions are imposed directly using both the displacement and cell tractions.

The current parametric HFGMC formulation with linear mapping employs full quadratic displacement expansion including the mixed bilinear term. This is an important difference because this term vanishes in the volumetric and surface integral based continuity applied in the previous HFGMC formulation using rectangular shaped cells. The need for full quadratic form of a displacement expansion emanates from the demand that the new mapping be applied to a general quadrilateral cell shape. As a result, additional moment equilibrium equations are needed in the current study in order to have sufficient equations for the added coefficients of expansion. The form of the average moment equilibrium is chosen by multiplying the pointwise stress based partial differential equations with the mixed bilinear coordinates before applying the average volume integration of the equations for each cell. This choice may not be the *optimal* one and further research may be needed to answer the question: What is the optimal equilibrium moment equation? Nevertheless, the performance and solution presented in the verification section indicates a more than

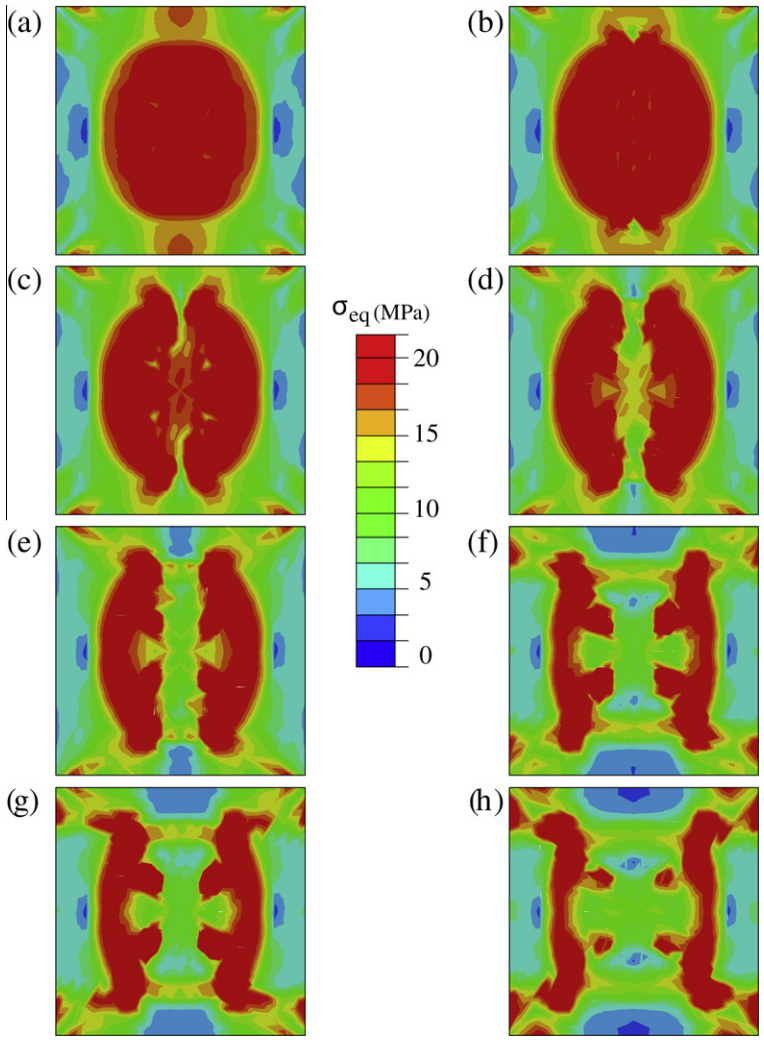

Fig. 12. Equivalent stress distribution sequence in the composite with the square array packing as predicted by the HFGMC with the cohesive fiber–matrix evolving damage.

adequate accuracy has been achieved by the current HFGMC formulation. This is despite the relatively smaller number of cells used to map complicated shape fibers and phases of the composite.

Finally, it is important to emphasize that the HFGMC can be used to generate refined micromechanical models when the aim is to evaluate the local spatial distributions in the phases in an accurate manner. Several other micromechanical models, e.g., Mori–Tanka, MOC, and the GMC, have been successfully applied to generate the effective stiffness and global nonlinear response of composite materials with high accuracy comparable to that of detailed FE models. These earlier micromechanical models have not accurately depict the fiber or phase geometry. In fact, it is clearly shown in these models that the exact shape of the fibers and their corresponding spatial distributions of deformation may not have dramatic effect on the effective stiffness or even the global nonlinear stress and strain. While the HFGMC can be used to obtain such accurate global solutions using very small number of cells, the ultimate goal is to propose using the HFGMC to generate the local distribution of deformation in the RUC when those are needed in addition to the macroscopic composite response. This point has been clearly demonstrated in the current study where local and global damage formulation was implemented within HFGMC. Thus, a refined micromechanical-damage approach is another justification for employing refined HFGMC micromechanical modeling. Damage derivation and implementation in this study indicate that this refined HFGMC coupled approach is well suited for predicting local (pointwise) or global (average) damage initiation and its subsequent progression. It should be mentioned that this is the first implementation of the proposed CED damage approach with the HFGMC method, and thus limited results have been presented. Future studies can further address various aspects of the micromechanical-damage coupling formulation.

6. Conclusions

A new micromechanical re-formulation of the HFGMC method is presented using parametric linear geometric mapping for the cells to allow modeling multiphase composites with arbitrary microstructural geometry. The displacement field and integration are performed in the auxiliary mapped parametric space while the overall original governing equations of the HFGMC remain intact. The use of general quadrilateral shaped cells necessitates the employment of a full quadratic polynomial form for the displacement field unlike the partial quadratic form used in the original HFGMC for rectangular cells. The new re-formulation allowed the use of a relatively few number of cells to capture the local stress fields especially at the fiber–matrix interfaces. The refined resolution of the HFGMC micromechanics allowed local damage formulation. This enabled a new cell extinction for progressive damage formulation where both local and global responses are generated within the proposed coupled micromechanical-damage formulation. The strain softening behavior and local load redistribution due to damage demand an iterative solution algorithm. The latter is proposed based on generating a proper residual form for the governing HFGMC equations and then used to iteratively update the damage and microvariables in order to satisfy the governing equations. Applications are presented to verify the HFGMC with linear mapping as compared with analytical and finite-element solutions. Two damage formulations (CED and cohesive models) have been coupled with the HFGMC to form a general micromechanical-damage framework. Limited progressive damage applications are also presented to demonstrate the ability to extend the HFGMC to damage without excessive computational cost. The new HFGMC formulation can be employed in a local–global framework for the general progressive damage analysis of composite structures.

Acknowledgment

The support from the Kahanoff Foundation and the European-Union Marie-Curie IRG grant are greatly acknowledged.

References

Aboudi, J., 1989. Micromechanical analysis of composites by the method of cells. Appl. Mech. Rev. 42, 193–221.
Aboudi, J., 1991. Mechanics of Composite Materials: A Unified Micromechanical Approach. Elsevier, Amsterdam.
Aboudi, J., 2001. Micromechanical analysis of fully coupled electro-magneto-thermo-elastic multiphase composites. Smart Mater. Struct. 10, 867–877.
Aboudi, J., 2002. Micromechanical analysis of the fully coupled finite thermo-elastic response of rubberlike matrix composites. Int. J. Solids Struct. 39, 2587–2612.
Aboudi, J., 2004. The generalized method of cells and high-fidelity generalized method of cells micromechanical models – a review. Mech. Adv. Mater. Struct. 11, 329–366.
Aboudi, J., 2005. Micromechanically established constitutive equations for multiphase materials with viscoelastic–viscoplastic phases. Mech. Time-Dependent Mater. 9, 121–145.
Aboudi, J., 2007. Micromechanical analyses of smart composite materials. In: Reece, P.L. (Ed.), Progress in Smart Materials and Structures. Nova Science Publishers, New York, pp. 291–361.
Aboudi, J., 2008. Finite strain micromechanical modeling of multiphase composites. Int. J. Multiscale Comput. Eng. 6, 411–434.
Aboudi, J., Gilat, R., 2005. Micromechanical analysis of lattice blocks. Int. J. Solids Struct. 42, 4372–4392.
Aboudi, J., Pindera, M.-J., Arnold, S.M., 2003. Higher-order theory for periodic multiphase materials with inelastic phases. Int. J. Plasticity 19, 805–847.
Allen, D.H., Jones, R.H., Boyd, J.G., 1994. Micromechanical analysis of a continuous fiber metal matrix composite including the effects of matrix viscoplasticity and evolving damage. J. Mech. Phys. Solids 42, 505–529.
Bansal, Y., Pindera, M.-J., 2004. Testing the predictive capability of the high-fidelity generalized method of cells using an efficient reformultation. NASA/CR-2004-213043.
Bansal, Y., Pindera, M.-J., 2006. Finite volume direct averaging micromechanics of heterogeneous materials with elastic–plastic phases. Int. J. Plasticity 22, 775–825.
Bednarcyk, B.A., Arnold, S.M., 2002. Transverse tensile and creep modeling of continuously reinforced titanium composites with local debonding. Int. J. Solids Struct. 39, 1987–2017.
Bednarcyk, B.A., Arnold, S.M., Aboudi, J., Pindera, M.-J., 2004. Local field effects in titanium matrix composites subject to fiber–matrix debonding. Int. J. Plasticity 20, 1707–1737.
Bednarcyk, B.A., Aboudi, J., Arnold, S.M., 2010. Micromechanics modeling of composites subjected to multiaxial progressive damage in the constituents. AIAA J. 48, 1367–1378.
Bednarcyk, B.A., Aboudi, J., Arnold, S.M., Sullivan, R.M., 2008. Analysis of space shuttle external tank spray-on foam insulation with internal pore pressure. J. Eng. Mat. Tech. 130, 041005–041016.
Boyd, J.G., Costanza, F., Allen, D.H., 1993. A micromechanics approach for constructing locally averaged damage dependent constitutive equations in inelastic composites. Int. J. Damage Mech. 2, 209–228.
Bruck, H.A., Gilat, R., Aboudi, J., Gershon, A.L., 2007. A new approach for optimizing the mechanical behavior of porous microstructures for pouros materials by design. Model. Simul. Mater. Sci. Eng. 15, 653–674.
Cook, R.D., Malkus, D.S., Plesha, M.E., Witt, R.J., 2002. Concepts and Applications of Finite Element Analysis. fourth ed., John Wiley, New York.
Camacho, G.T., Ortiz, M., 1996. Computational modeling of impact damage in brittle materials. Int. J. Solids Struct. 33, 2899–2938.
Chow, C.L., Lu, T.J., 1989. On evolution laws of anisotropic damage. Eng. Fract. Mech. 34, 679–701.
Freed, Y., Aboudi, J., 2009. Micromechanical prediction of the two-way shape memory effect in shape memory composites. Int. J. Solids Struct. 46, 1634–1647.
Haj-Ali, R., Aboudi, J., 2009. Nonlinear micromechanical formulation of the high fidelity generalized method of cells. Int. J. Solids Struct. 46, 2577–2592.
Haj-Ali, R., El-Hajjar, R.F., Muliana, A.H., 2006. Cohesive fracture modeling of crack growth in thick-section composites. Eng. Fract. Mech. 73, 2192–2209.
Haj-Ali, R.M., 2009. Cohesive micromechanics: a new approach for progressive damage modeling in laminated composites. Int. J. Damage Mech. 18, 691–719.
Haj-Ali, R., 2008. Nested nonlinear multiscale frameworks for the analysis of thick-section composite materials and structures. In: Kwon, Y.W., Allen, D.H., Talreja, R. (Eds.), Multiscale Modeling and Simulation of Composite Materials and Structures. Springer, New York, pp. 332–371.
Kachanov, L., 1986. Introduction to Continuum Damage Mechanics. Springer.
Khatam, H., Pindera, M.-J., 2009. Parametric finite-volume micromechanics of periodic materials with elastoplastic phases. Int. J. Plasticity 25, 1386–1411.
Krajcinovic, D., 1996. Damage Mechanics. North-Holland Series in Applied Mathematics and Mechanics. North Holland.
Lemaitre, J., 1996. A Course on Damage Mechanics. Springer, New York.
Lemaitre, J., Desmorat, R., 2005. Engineering Damage Mechanics. Springer, Berlin.

Lemaitre, J., Chaboche, J.L., 1990. Mechanics of Solid Materials. Cambridge University Press, Cambridge.
Majumdar, B.S., Newaz, G.M., Ellis, J.R., 1993. Evolution of damage and plasticity in titanium based fiber reinforced composites. Metall. Trans. 24A, 1597–1610.
Matzenmiller, A., Lubliner, J., Taylor, R.L., 1995. A constitutive model for anisotropic damage in fiber-composites. Mech. Mater. 20, 125–152.
Mura, T., 1987. Micromechanics of Defects in Solids. second ed., Springer.
Muskhelishvili, N.I., 1963. Some Basic Problems of the Mathematical Theory of Elasticity: Fundamental Equations, Plane Theory of Elasticity, Torsion and Bending, Groningen, The Netherlands, Noordhoff.
Paley, M., Aboudi, J., 1992. Micromechanical analysis of composites by the generalized cells model. Mech. Mater. 14, 127–139.
Ryvkin, M., Aboudi, J., 2007. The effect of fiber loss in periodic composites. Int. J. Solids Struct. 44, 3497–3513.
Talreja, R., 1985a. A continuum mechanics characterization of damage in composite materials. Proc. R. Soc. A, 195–216.
Talreja, R., 1985b. Transverse cracking and stiffness reduction in composite laminates. J. Compos. Mater. 19, 355–375.
Talreja, R., 1994. Damage Mechanics of Composite Materials, vol. 1. Elsevier Science.
Voyiadjis, G.Z., 1993. Damage in Composite Materials. Elsevier Publishing Company.
Voyiadjis, G.Z., Allen, D.H., 1996. Damage and Interfacial Debonding in Composites. Studies in Applied Mechanics. Elsevier Science.
Voyiadjis, G.Z., Deliktas, B., 1997. Damage in MMCs using the GCM: theoretical formulation. Compos. B 28B, 597–611.
Voyiadjis, G.Z., Kattan, P.I., 1999. Advances in Damage Mechanics: Metal and Metal Matrix Composites. Elsevier, Amsterdam.
Voyiadjis, G.Z., Kattan, P.I., 2005. Damage Mechanics. Taylor & Francis, Boca Raton, FL.